

Accurate Hellmann–Feynman forces with optimized atom-centered Gaussian basis sets in density functional theory

Shivesh Pathak,^{1, a)} Ignacio Ema López,² Alex J. Lee,³ William P. Bricker,³ Rafael López Fernández,² Susi Lehtola,^{4, 5} and Joshua A. Rackers¹

¹⁾Center for Computing Research, Sandia National Laboratories

²⁾Departamento de Química Física Aplicada, Universidad Autónoma de Madrid

³⁾Department of Chemical and Biological Engineering, University of New Mexico

⁴⁾Molecular Sciences Software Institute, Virginia Tech

⁵⁾Department of Chemistry, University of Helsinki

The Hellmann–Feynman (HF) theorem provides a way to compute forces directly from the electron density, enabling efficient force calculations for large systems through machine learning (ML) models for the electron density. The primary issue holding back the general acceptance of the HF approach for atom-centered basis sets is the well-known Pulay force which, if naively discarded, typically constitutes an error upwards of 10 eV/Å in forces. In this work, we construct specialized atom-centered Gaussian basis sets to reduce the Pulay force: the σ NZHF (N = Single, Double, Triple) basis sets. We demonstrate these basis sets' effectiveness in computing accurate HF forces within density functional theory and find that HF forces computed using the double- ζ (N = D) and triple- ζ (N = T) basis sets yield comparable accuracy to analytic forces computed using size matched pcseg-N and aug-pcseg-N basis sets for typical benchmark molecules and DNA fragments. We also find that geometry optimization and molecular dynamics using HF forces with the σ DZHF basis yield comparable results to calculations run with analytic forces and the size-matched pcseg-2 basis. Our results illustrate that the σ NZHF basis sets yield HF forces with state-of-the-art accuracy appropriate for applications like geometry optimization and molecular dynamics, paving a clear path forwards for accurate and efficient simulation of large systems using the HF theorem and ML densities.

I. INTRODUCTION

A pressing issue in contemporary materials simulations is the accurate and efficient first principles calculation of atomic forces in large systems. A representative class of such materials are protein molecules—some containing beyond 100,000 atoms—where accurate forces would allow for advancements in the understanding of processes such as protein folding.^{1–7} Regarding periodic systems, materials with computational unit cells surpassing tens of thousands of atoms remain a challenge, while accurate simulation of the correlated electronic structure of van der Waals materials like twisted bilayer graphene would require force calculations on superlattices surpassing 40,000 atoms.^{8–11} Even with adaptations for increased efficiency,^{12–14} the most commonly used first principles method, density functional theory^{15,16} (DFT), is unable to efficiently and accurately compute forces for such large-scale systems.

Machine learning (ML) has recently emerged as an effective solution to the seemingly intractable problem of accurate computation of properties of large systems. The effectiveness of ML methods stems from their ability to extrapolate solutions from simple training data to more complex use cases: traditional first principles methods are only needed for generating the training data for the ML model, while the systems to which the ML techniques are eventually applied are typically orders of magnitude larger than the training configurations. ML models are

able to predict properties such as hopping parameters,⁸ potential energy surfaces, as well as forces^{17–19} for large molecules and complicated solids.

While ML models are routinely trained to compute forces directly,¹⁷ the Hellmann–Feynman (HF) theorem presents a promising alternative approach. Under the Born–Oppenheimer (BO) approximation, the analytic expression for the force acting on nucleus I situated at \vec{R}_I is²⁰

$$\vec{F}_I^E = -\frac{\partial E}{\partial \vec{R}_I} = -\frac{\partial \langle \Psi(\{\vec{R}\}) | \hat{H} | \Psi(\{\vec{R}\}) \rangle}{\partial \vec{R}_I} = \vec{F}_I^{\text{HF}} + \vec{F}_I^{\text{Pulay}}, \quad (1)$$

where the HF term is

$$\vec{F}_I^{\text{HF}} = -\left\langle \Psi(\{\vec{R}\}) \left| \frac{\partial \hat{H}}{\partial \vec{R}_I} \right| \Psi(\{\vec{R}\}) \right\rangle \quad (2)$$

and the Pulay term²⁰ originating from the geometry dependence of the basis set used to represent the electronic wave function $|\Psi\rangle$ is

$$\vec{F}_I^{\text{Pulay}} = -2 \left\langle \Psi(\{\vec{R}\}) \left| \hat{H} \left| \frac{\partial \Psi(\{\vec{R}\})}{\partial \vec{R}_I} \right. \right| \Psi(\{\vec{R}\}) \right\rangle, \quad (3)$$

where $\{\vec{R}\}$ is the set of all nuclear positions and \hat{H} is the electronic Hamiltonian. It is important to point out here that if $|\Psi\rangle$ is numerically exact, that is, if it is computed at the complete basis set (CBS) limit, the Pulay force of Eq. 3 vanishes and the analytic force equals the HF force.

Now, the only terms in the electronic Hamiltonian that depend on the nuclear coordinates $\{\vec{R}\}$ are nuclear-

^{a)}Electronic mail: sapatha@sandia.gov

nuclear repulsion

$$\hat{H}^{\text{nuc-nuc}} = \sum_{IJ} \frac{Z_I Z_J}{|\vec{R}_I - \vec{R}_J|} \quad (4)$$

and nuclear-electron attraction

$$\hat{H}^{\text{nuc-el}} = - \sum_I Z_I \int \frac{\rho(\vec{r})}{|\vec{r} - \vec{R}_I|} d^3r, \quad (5)$$

where Z_I is the atomic number of nucleus I . As these are the only terms that contribute to Eq. 2, the HF force can be computed at the basis solely on the knowledge of the electron density ρ .

At the CBS limit, the analytic force reduces to the HF force, and thereby we only need knowledge of the electron density ρ to evaluate forces acting on the nuclei. Making use of the HF theorem, an ML model which predicts accurate, that is, near-CBS electron densities could thereby yield accurate forces on large scale systems, at considerably smaller cost than an ML model for forces, since the training data would be much simpler to generate.^{21,22}

The only remaining question is: How do we get close enough to the CBS limit to allow such modeling? If the Pulay force of Eq. 3 can be sufficiently suppressed, using the HF force of Eq. 2 in place of the analytic force of Eq. 1 would amount to negligible error.

Perhaps the earliest musings on reducing Pulay forces was by Pulay himself in ref. 23, where he noted that the HF forces could be accurately computed using fixed basis functions if the basis could accurately describe the derivatives of the wave functions $|\partial\Psi/\partial\vec{R}_I\rangle$.

A few years later, Nakatsuji and coworkers^{24–26} began constructing such basis sets, where derivatives of the basis functions were included in the orbital basis. The resulting "family" style basis sets were found to yield reasonably accurate HF forces, equilibrium geometries, and force constants for small molecules.

However, Pulay levied criticism on this approach²⁷ for (i) the computational expense of including large numbers of core polarization functions that are necessary for accurate HF forces²³ as well as (ii) the poor accuracy of the approach of Nakatsuji and coworkers for molecular geometries compared to standard basis sets with the analytical derivative approach. Nakatsuji *et al.* rebutted the criticism by stating that even though the computational costs are higher, the results are more easy to interpret chemically thanks to the fulfillment of the HF theorem.²⁸

Pulay's views have been since widely adopted by the quantum chemistry community: HF forces have practically vanished from consideration. However, it is important to note that the pioneering studies by Pulay and Nakatsuji and coworkers were limited to tiny basis sets due to the meager computational resources available at the dawn of quantum chemistry. Small basis sets are known to be unreliable for chemical applications. Even if the Pulay term of Eq. 3 is suppressed in such a basis, the electron density ρ may still have large errors, which

lead to large errors in the HF force, as well. Modern applications of quantum chemistry routinely use extended basis sets of polarized triple- ζ quality or higher, which were not tractable at the time of the early studies of Pulay, Nakatsuji and coworkers; the applicability of the old ideas of Pulay, Nakatsuji and coworkers thus deserve revisiting. Even though geometry optimization was pursued in the early works referenced above,^{24–28} the studies were limited to small basis sets and the larger basis sets that are routinely used nowadays should lead to more reliable HF forces and geometries.

Much more recently, Rico *et al.*²⁹ proposed a new "family" style basis set for Slater-type orbitals with preliminary tests demonstrating noticeably attenuated Pulay forces and accurate electronic structures without the excessive overheads suggested by Pulay. Unresolved by Rico *et al.*, however, are the questions of scalability and applicability of these forces in applications like geometry optimization and molecular dynamics. In this work, we follow Rico *et al.* and demonstrate that specially optimized atom-centered Gaussian basis sets yield HF forces with an accuracy comparable to analytic forces computed with state-of-the-art Gaussian basis sets within DFT, and that they can be used to get state-of-the-art accuracy in applications of geometry optimization and molecular dynamics.

The organization of this work is the following. In section II, we construct a series of basis sets dubbed σ NZHF (N = Single, Double, Triple) that are optimized to reduce the Pulay term in Eq. 1. Section III includes computational details for DFT, as well as geometry optimization and molecular dynamics (MD) methods employed in the rest of the manuscript, followed by the results of these computations in section IV. We finish in section V with a short summary and conclusions.

The organization of the results, section IV, is as follows. We begin the demonstration of the accuracy of HF forces by computing force curves for the CO molecule in section IV A. In section IV B, we carry out an in-depth analysis of total energies, analytical forces, and HF forces over a standard benchmark set of molecules,³⁰ and follow-up with a similar analysis for DNA fragments in section IV C. Our results show that the HF forces computed using the σ DZHF and σ TZHF basis sets yield similar accuracy to analytical forces computed using the size-matched σ NZ³¹ and (aug-)pcseg-N³² basis sets. With this in mind, we follow up in section IV D with a study of geometry optimization on the benchmark molecule set of ref. 30 in section IV B, finding that optimizing geometries with HF forces with the σ DZHF basis yields less than 1% error compared to geometries optimized with analytic forces and the size-matched pcseg-2 basis. As a final application of our basis set, we conduct a 100 fs room-temperature Born–Oppenheimer molecular dynamics (BOMD) calculation on a single ethanol molecule using HF forces and the σ DZHF basis in section IV E, finding excellent agreement in both total energies and configurations when compared to a BOMD calculation

TABLE I. Number of primitive and contracted basis functions for the σ NZ³¹ and σ NZHF (this work) basis sets for the considered first row and second row atoms. N_{exp} denotes the number of unique exponents in the basis set.

Basis	N_{exp}	# Primitives	# Contracted
H atom			
σ SZ	10	10 (10s)	1 [1s]
σ DZ	10	19 (10s, 3p)	5 [2s, 1p]
σ TZ	10	37 (10s, 4p, 3d)	14 [3s, 2p, 1d]
σ SZHF	10	40 (10s, 10p)	4 [1s, 1p]
σ DZHF	10	55 (10s, 10p, 3d)	17 [3s, 3p, 1d]
σ TZHF	12	85 (11s, 11p, 4d, 3f)	46 [6s, 6p, 3d, 1f]
C, N, O and F atoms			
σ SZ	15	45 (15s, 10p)	5 [2s, 1p]
σ DZ	15	60 (15s, 10p, 3d)	14 [3s, 2p, 1d]
σ TZ	15	86 (15s, 10p, 4d, 3f)	30 [4s, 3p, 2d, 1f]
σ SZHF	15	110 (15s, 15p, 10d)	17 [3s, 3p, 1d]
σ DZHF	15	131 (15s, 15p, 10d, 3f)	46 [6s, 6p, 3d, 1f]
σ TZHF	17	169 (16s, 16p, 10d, 4f, 3g)	87 [8s, 8p, 5d, 3f, 1g]
P, S and Cl atoms			
σ SZ	19	79 (19s, 15p)	9 [3s, 2p]
σ DZ	19	79 (19s, 15p, 3d)	18 [4s, 3p, 1d]
σ TZ	19	95 (19s, 15p, 4d, 3f)	34 [5s, 4p, 2d, 1f]
σ SZHF	19	113 (19s, 19p, 15d)	30 [5s, 5p, 2d]
σ DZHF	19	134 (19s, 19p, 15d, 3f)	59 [8s, 8p, 4d, 1f]
σ TZHF	21	187 (20s, 20p, 15d, 4f, 3g)	100 [10s, 10p, 6d, 3f, 1g]

run with analytic forces computed using the pcseg-2 basis.

II. HELLMANN–FEYNMAN OPTIMIZED BASIS SET

We follow the strategy of Rico et al.²⁹ to construct the HF optimized basis sets by iteratively improving an initial basis set to reduce the error Δ_λ in the basis set projection of the nuclear forces of the basis functions, see Eq. 6 of ref. 29. More functions are added into the basis set, until the error is suitably small as determined by a parameter ϵ , $\Delta_\lambda < \epsilon$. As a result of this procedure, the Pulay forces are reduced to the order of ϵ . Below we provide a sufficient overview of the basis set construction procedure for the reader, with additional implementation details in the Supplementary Material.

We start from the family-style *sigma* basis sets of Ema et al.³¹ (σ NZ, N = Single, Double, Triple). The σ NZ basis sets have been optimized following the general lines of the procedure of Dunning³³ by minimizing the configuration interaction singles and doubles (CISD) energy of gas-phase atoms.³¹ The composition of the σ NZ basis sets is shown in Tab. I. The σ NZ basis sets were chosen as the starting point of this work, as the σ NZ basis sets consist of contractions of primitive Gaussian-type orbitals (pGTOs) whose exponents are shared by several angular momenta: if a given primitive appears multiplied by a spherical harmonic of quantum number $l = L$, analogous functions with the same exponent are also present for $0 \leq l < L$. The use of shared exponents results in the inclusion of a great deal of the derivative space in the basis, simplifying the efforts of this work.

To develop a basis with a high degree of fulfillment of the HF theorem, we extend the σ NZ basis sets with functions corresponding to the occupied basis functions' derivatives. As shown in Eq. 16 of the Supplementary Material, the derivative of a pGTO with a given $l > 0$ yields three functions with the same exponent as in the pGTO: one function corresponding to $l + 1$, another to $l - 1$, and one function to $l - 1$ but bearing an additional factor r^2 . As the present basis sets employ spherical functions only, the radial factors included in the pGTOs for angular momentum l is r^l . Because of this, we remove the additional functions with r^2 from consideration, yielding what we call a *reduced set of primitives* that span the *reduced space*.

Our goal is to iteratively improve the *reduced space* so that the distance between it and the *reference space*—the space spanned by contractions of σ NZ and their derivatives—becomes smaller than the used threshold $\epsilon = 10^{-3}$. The procedure proceeds as follows.

0. Choose the initial basis set, yielding a *reduced space* and a *reference space*.
1. Compute Δ_λ with the given reduced space and reference space.
2. If $\Delta_\lambda < \epsilon$, stop.
3. Otherwise, add additional primitive functions to the reduced set and go back to step 1.

Details on computing Δ_λ for Gaussian basis functions as well as the decision criteria for exponents and angular momenta of the added pGTOs can be found in Sections 2–5 of the Supplementary Material.

Once the improved *reduced set of primitives* has been formed, we carry out an expansion of the functions of the *reference set* in an orthogonal basis of the *reduced set of primitives* to form the final contracted σ NZHF basis sets. We find that projecting into the full *reduced set of primitives* is generally unnecessary. Rather, by choosing a suitable subspace of the *reduced space* to project into, we can reduce the number of final contracted basis functions in σ NZHF up to 20% for heavier atoms. Details of the iterative approach for finding a suitable subspace can be found in Section 5 of the Supplementary Material.

The σ NZHF basis sets resulting from this procedure are the final HF basis sets used in this work. The compositions of the σ NZHF basis sets are shown in Tab. I in terms of primitive and contracted functions; the compositions of the original σ NZ basis sets are also included for comparison. It should be noted that additional pGTOs (namely, *s* and *p* primitives) were only required for the σ TZHF basis sets. The σ NZHF basis sets for H, C, N, O, F, P, S and Cl are provided in the Supplementary Material and can be found on the Basis Set Exchange^{34,35}.

III. COMPUTATIONAL DETAILS

We compute forces from first principles to conduct geometry optimization and carry out BOMD simulations for a wide range of molecular systems. The electronic first principles problem is solved using DFT with the PBE0 functional^{36,37} from Libxc³⁸. DFT calculations in sections IV A, IV B and IV C were carried out with a custom version of the Psi4 package³⁹ available at <https://github.com/JoshRackers/psi4>, while all other DFT calculations were done using the PySCF package^{40,41}. Density fitting was employed with the def2-universal-jkfit auxiliary basis of Weigend⁴². A (75, 302) quadrature grid for the DFT functional was used for all atoms in Psi4, and all atoms except hydrogen in PySCF, for which a (50, 302) quadrature grid was used instead.

Geometry optimization was carried out using the geometricTRIC⁴³ solver within PySCF. We use the default geometricTRIC convergence criteria for optimization, namely a energy convergence criterion of $10^{-6}E_h$, force maximum and RMS values of $3 \times 10^{-4}E_h/a_0$ and $4.5 \times 10^{-4}E_h/a_0$, respectively, with a_0 the Bohr radius and configuration deviation maximum and RMS values of 1.2×10^{-3} Å and 1.8×10^{-3} Å, respectively. BOMD calculations are carried out in the NVE ensemble, also within the PySCF package. The Verlet integrator⁴⁴ is used out to a final time of 100 fs using 1 fs time steps, and an initial randomized velocity is given to the system to maintain a time-averaged temperature ~ 300 K. For clarity, we note that when HF forces are employed for optimization, convergence criteria such as the force maximum and RMS force refer to the computed HF forces; when using HF forces for MD, all accelerations are computed using HF forces only.

IV. RESULTS

A. Diatomic force curve for CO

We begin by computing a force curve for the CO molecule as a simple demonstration of the accuracy of HF forces in DFT using the σ NZHF basis, shown in Fig. 1; this molecule was also examined by Nakatsuji et al.²⁶ with Hartree-Fock and small Pople-style basis sets. To understand the effect of the added basis functions to fulfill the HF theorem, we also compute analytic and HF forces using the σ NZ basis sets that were the starting point for the σ NZHF basis sets. Furthermore, to make a fair comparison to the state-of-the-art in basis set development, we computed energies and forces using size-matched pcseg-N basis sets³² that are optimized for accurate DFT total energies. A reference curve computed using the analytic force and the pcseg-4 basis set is also shown in each panel. As a point of reference, Tab. II presents the comparison of basis set sizes for the σ NZHF, σ NZ and pcseg-N basis sets for a single CO molecule.

We begin by comparing the HF force computed using

the σ NZ, σ NZHF, and pcseg-N basis sets over the benchmark molecule set, shown in the first row of Fig. 1. Large deviations from the reference forces can be observed in the results obtained with the σ NZ and pcseg-N basis sets. These large differences arise from the unsuitability of standard basis sets for computing HF forces: even the quadruple- ζ pcseg-3 basis set (shown in the rightmost column) exhibits considerable errors in the HF force. In contrast, we find that the σ NZHF basis sets of this work yield force curves which agree well with the reference calculation. While the curve computed with the σ SZHF basis set differs visually from the reference curve for reasons discussed in the following paragraph, the σ DZHF and σ TZHF curves are in excellent agreement with the reference data. These results demonstrate the efficacy of the optimized σ NZHF sets of this work in reducing the Pulay forces.

Analytic forces are compared in the second row of Fig. 1. The larger σ DZHF and σ TZHF basis sets again yield good agreement with the reference calculation, and afford similar accuracy to the size-matched pcseg-N basis sets that have been designed for DFT calculations. The smallest basis set σ SZHF, however, yields larger errors than pcseg-1 when computing analytic derivatives.

The comparison of the HF and analytic forces for σ SZHF, shown in the upper and lower panels of the leftmost column of Fig. 1, respectively, shows that the HF force is an accurate approximation of the analytic gradient in the σ SZHF basis set, that is, the Pulay forces have been successfully made negligible by the design of the basis set. Combined with the inaccuracy of the analytic gradient in the σ SZHF calculation, this indicates that the σ SZHF basis set is simply too small for quantitative electronic structure calculations, like its parent, the minimal σ SZ basis set. The error in the HF force arises mostly from the limitations in the description of the electron density in the small basis set, as discussed in the Introduction.

Although data for σ SZHF basis sets is included throughout this work as a point of reference, σ SZHF results will not be discussed in the remainder of this work, as the same remarks on the inherently limited accuracy of small basis sets apply throughout the discussion. The larger σ DZHF and σ TZHF basis sets, however, not only provide accurate analytical gradients, but are also useful for HF force calculations. These results illuminate the pivotal difference between the pioneering attempts at HF forces in the literature²⁴⁻²⁸ and the approaches pursued in this work: although small basis sets only afford results of limited quality, larger basis sets allow the reproduction of accurate HF forces while still being compact enough to enable routine calculations on existing computing platforms.

As a last point we discuss the total force acting on the system, $\vec{F}_{\text{tot}} = (\vec{F}_C + \vec{F}_O)$, which should be zero for a calculation with no external forces. The analytic DFT force calculations will not have exactly vanishing total force, as the finite integration grid for the DFT functional breaks

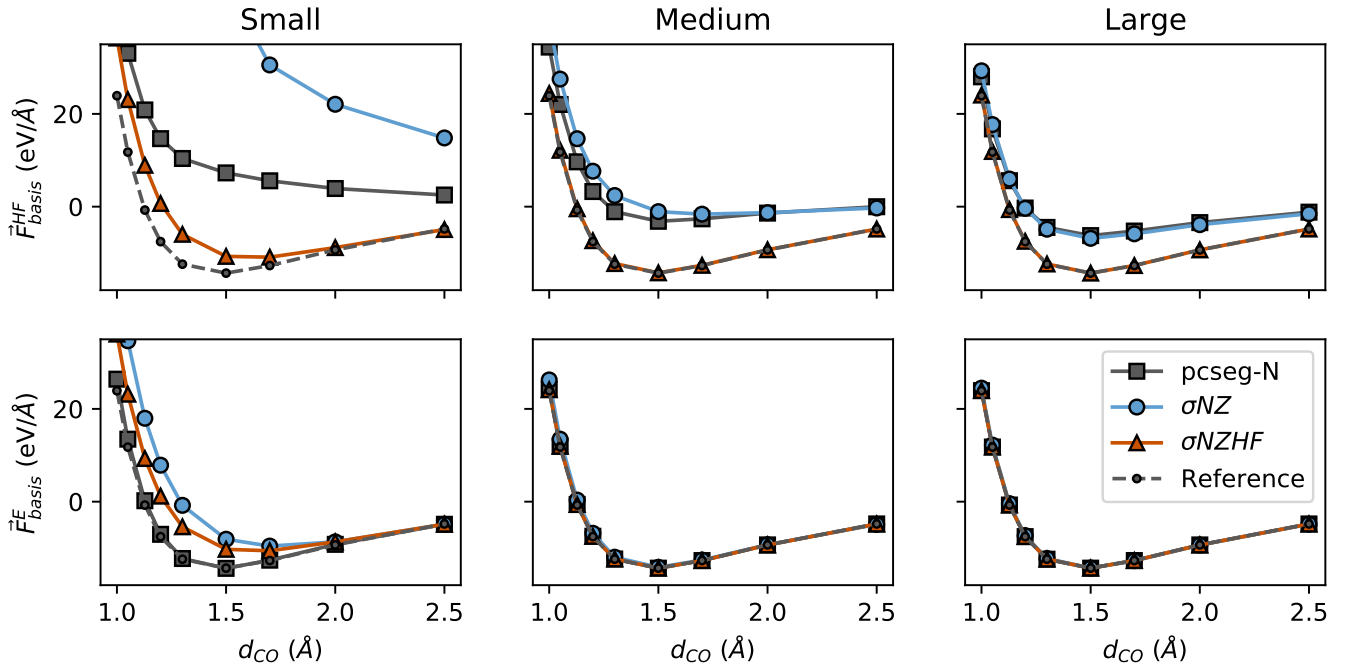


FIG. 1. Diatomic force curves for CO molecule computed as a function of bond length d_{CO} . The force shown is the force along the bond, namely $\vec{F}_{CO} = (\vec{F}_C - \vec{F}_O)/2$. Columns are delineated by the basis set size classified within Tab. II, and rows by the force computed: analytic or HF. The dashed Reference curve is a reference calculation for the reader, computed using the large pcseg-4 basis and analytic forces.

continuous spatial translation symmetry and thereby total momentum conservation is lost. HF forces computed within DFT will suffer from the same issue, compounded with the fact that discarding the Pulay force of Eq. 3, no matter how small, will lead to an additional systematic error in the total force. For analytic forces computed with the pcseg-3 basis we find $|\vec{F}_{tot}| \sim 10^{-5}$ eV/Å, while for HF forces computed with the σ TZHF basis, we find $|\vec{F}_{tot}| \sim 10^{-3}$ eV/Å. We believe that both of these total force magnitudes are sufficiently small for practical and accurate force calculations. We would also like to note that errors in the HF forces introduced by discarding the suppressed Pulay force cannot break discrete symmetries of molecular systems, unless the electron density used to compute the HF force also breaks the symmetry. For example, this ensures that out-of-plane forces for planar molecules always vanish, unless the electron density breaks the planar symmetry by an asymmetry around the plane.

B. Force comparison at fixed geometries of a benchmark set

We follow up our force curve demonstration with a more robust analysis of force errors over a benchmark set of small- to medium-size organic molecules taken from Baker's seminal work on geometry optimization.³⁰ In this study we consider eight molecules from the bench-

Category	Basis	Size	Basis	Size	Basis	Size
Small	σ SZ	10	σ SZHF	34	pcseg-1	28
Medium	σ DZ	28	σ DZHF	92	pcseg-2	60
Large	σ TZ	60	σ TZHF	174	pcseg-3	120
Reference					pcseg-4	202

TABLE II. Comparison of basis set sizes for a single CO molecule. The σ NZHF series of this work are contrasted to the σ NZ and pcseg-N series used in this work. The "Small," "Medium," and "Large" categories are used in this work for comparison between various basis sets of similar size.

mark set: water, ammonia, ethane, acetylene, allene, methylamine, hydroxysulphane, and ethanol. For each molecule, the non-equilibrium configurations stated as "starting configurations" in Baker's work are used to compute HF forces, analytic forces and total energies.

We begin by comparing the HF force computed using the σ NZ, σ NZHF, and pcseg-N basis sets over the benchmark set. The errors in the HF forces (\vec{F}_{basis}^HF) compared to analytic forces computed in the pcseg-4 basis (\vec{F}_{ref}^E) are shown in the first panel of each sub-figure of Fig. 2. Since one force vector is obtained for each atomic center in the molecule, the distribution of force errors is visualized by bars that covers the range of errors from maximum to minimum over all the atoms in the molecule.

We find that the σ DZHF and σ TZHF basis sets yield HF forces with errors that are nearly two orders of magnitude smaller than those of the similarly sized σ NZ and

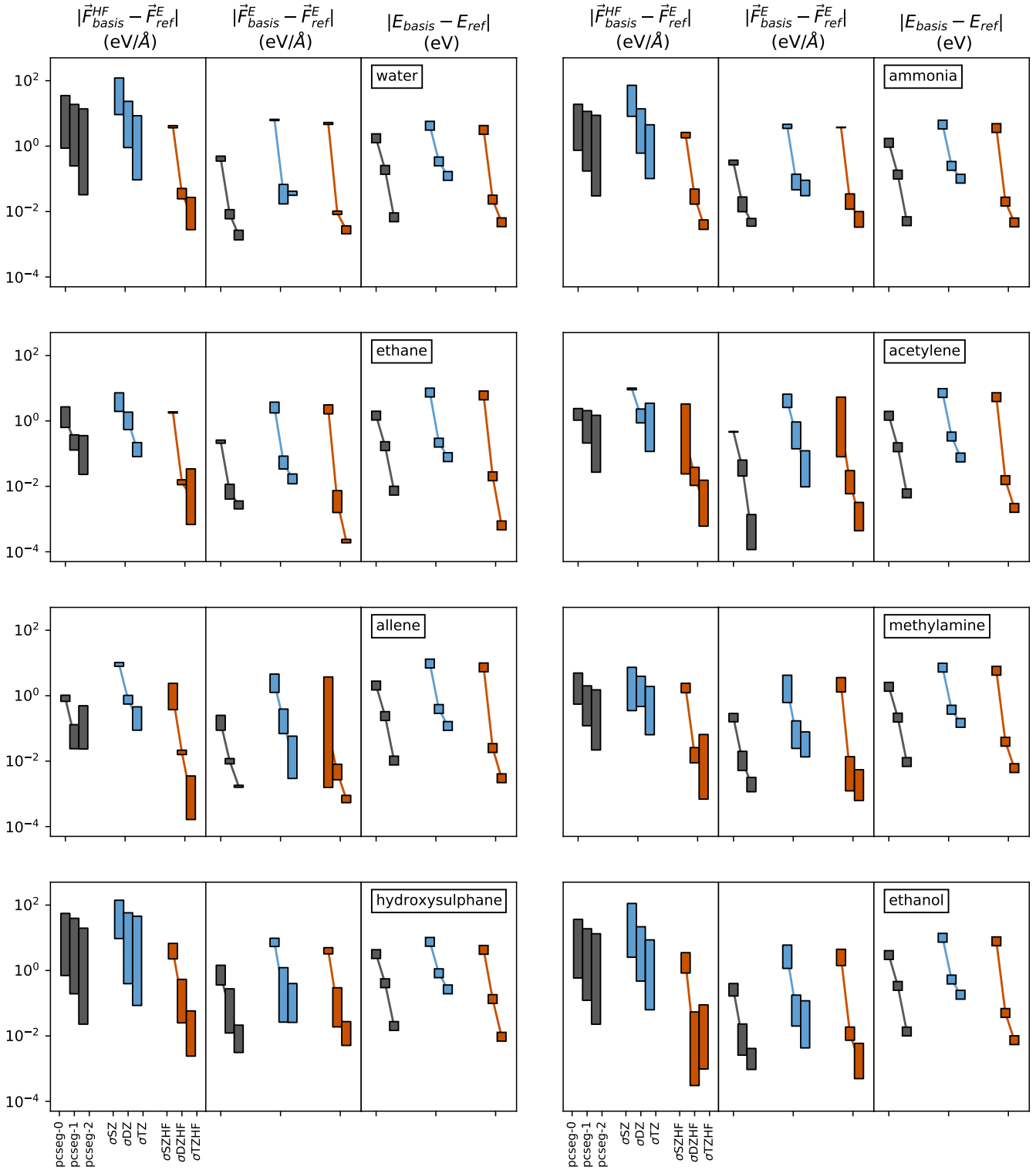


FIG. 2. Comparison of HF forces, analytic forces, and total energies for various small- to medium-size benchmark molecules. Each set of three panels are data for a particular molecule, with one panel for each physical quantity computed. The x-axis denotes the basis set used in the calculation, namely the three basis series with Small, Medium and Large sets defined in Tab. II. Since force vectors are computed on each atomic center of a given molecule, this results in multiple data points per force calculation; these points are represented by bars denoting the range of the force errors. In contrast, there is only one total energy per molecule. Absolute errors are plotted relative to analytic forces and energies computed using the pcseg-4 basis.

pcseg-N basis sets, once again demonstrating the ability of the σ NZHF basis sets to reduce Pulay forces. The poorer performance of σ SZHF can again be attributed to its insufficient size, as discussed in section IV A, and its results will not be discussed in detail.

Analytic forces are compared in the second panel of each sub-figure in Fig. 2. The larger σ DZHF and σ TZHF basis sets once again afford a 5-fold to 10-fold reduction in the force error relative to the σ NZ, and similar accuracy to the pcseg-N basis sets which have been designed for DFT calculations. A further important point is the ability of the σ NZHF basis sets in computing the total energy; these results are presented in the third panel of the sub-figures of Fig. 2. The σ NZHF basis sets yield fast convergence to the basis set limit with an accuracy that is surprisingly similar to or even better than that of the pcseg-N basis sets that have been optimized for DFT calculations.

The two largest σ NZHF (and pcseg-N) basis sets both afford errors 1–2 orders of magnitudes smaller than the similarly sized σ NZ basis sets. This is somewhat surprising, given that the σ NZHF basis sets are generated from the σ NZ basis sets by inclusion of basis function derivatives. Apparently, the inclusion of such derivatives leads to considerable improvements in the accuracy of DFT total energies, in addition to better satisfaction of the HF theorem. The HF basis sets may thus be useful for accurate computations of total energies and analytical derivatives, as well.

C. Force comparison at fixed geometries on DNA fragments

As a final demonstration of the accuracy of HF forces using the σ NZHF basis set, we computed HF and analytical forces on small DNA fragments. DNA fragments are formed of more elements than present in the benchmark set of section IV B, containing P atoms in addition to H, C, N and O. Therefore, the DNA calculations allow us to determine the accuracy of HF forces computed with the σ NZHF basis sets in a system containing second row atoms.

DNA fragment geometries were obtained from MD simulations performed in a previous study⁴⁵ using the Amber 20 package⁴⁶ and the BSC1 force field⁴⁷. DNA was modeled as 12 base pair strands (“12-mers”) in the canonical B-form⁴⁸, the most common structural form of DNA. To ensure adequate sampling of DNA’s conformational space, MD simulations were run on four different 12-mer base sequences.

Solvent molecules were modeled explicitly as TIP3P water⁴⁹ with a Mg^{2+} and Cl^- counterion concentration of about 100 mmol/L.

Initial DNA structures were first minimized and then allowed to heat up from 0 K to 300 K for 40 ps. After heating, 50 ns production runs were performed in the NPT ensemble at 1 atm and 300 K. We used the

Langevin thermostat with a collision frequency of 1 ps⁻¹, the Berendsen barostat with a relaxation time of 2 ps, and a time step of 2 fs. For each DNA structure, three simulations were performed with different starting trajectories for a combined simulation time of 150 ns. Fragment geometries were constructed from production run snapshots by extracting the central two base pairs of the 12-mer sequence and stripping away the rest of the molecule.

From the MD snapshots of DNA configurations, we analyzed ten configurations of six types of DNA fragments for a total of 60 structures. The six fragments include the four nucleotides (base + sugar + phosphate) with each of the bases (A, C, G, and T), and the two base pair structures (A-T and C-G), each fragment containing around 35 atoms. Note that the nucleotides are negatively charged due to the phosphate group whereas the base pair structures are neutral.

A comparison of the HF forces with the σ DZHF basis ($\vec{F}_{\sigma DZHF}^{HF}$) and analytical forces in the σ DZHF, pcseg-2 and aug-pcseg-2 basis sets (\vec{F}_{basis}^E) against reference analytical forces in the aug-pcseg-3 basis set ($\vec{F}_{\text{aug-pcseg-3}}^E$) is shown in Fig. 3. The distribution of force errors pertaining to the multiple studied configurations is shown with standard box plots, where the box indicates the first to third quantiles, the whiskers denote 90% confidence interval, and the center line denotes the median error.

We begin by noting that there is little difference between the errors in the pcseg-2 and aug-pcseg-2 analytical forces. The lack of difference is likely due to the non-equilibrium nature of the DNA MD samples, which had 26 meV additional energy per mode, washing out the importance of diffuse functions in describing the electronic structure. In contrast to our results, equilibrium calculations on DNA have indicated the importance of diffuse functions particularly in describing the ionic phosphate group.^{50,51} Due to the negligible difference between the pcseg-2 and aug-pcseg-2 forces on our non-equilibrium configurations, we limit the discussion of force errors to the σ DZHF and pcseg-2 basis sets.

We find excellent agreement for forces computed with the σ DZHF and pcseg-2 basis sets across all atomic species. Analytic forces computed with σ DZHF have comparable error to those computed with pcseg-2, while σ DZHF HF forces have slightly larger errors than pcseg-2 analytic forces. To quantify the larger errors present in the HF force calculations, we compute the increase in the median errors shown in Fig. 3 relative to the pcseg-2 analytic forces. For the H, C, N, O and P atoms, we find the median errors for the σ DZHF HF forces are larger by a multiplicative factor of 1.5, 1.8, 1.6, 1.1 and 1.9 relative to the pcseg-2 analytic forces—all below a factor of 2. As the quality of the σ NZHF basis set is contingent on the quality of the starting basis set, systematic improvements to the HF error can be pursued by beginning with a higher quality starting basis set than the σ NZ bases used in this work. Especially, the σ NZ basis sets have been optimized for atomic CISD energies; starting from a basis set optimized for DFT energies would likely

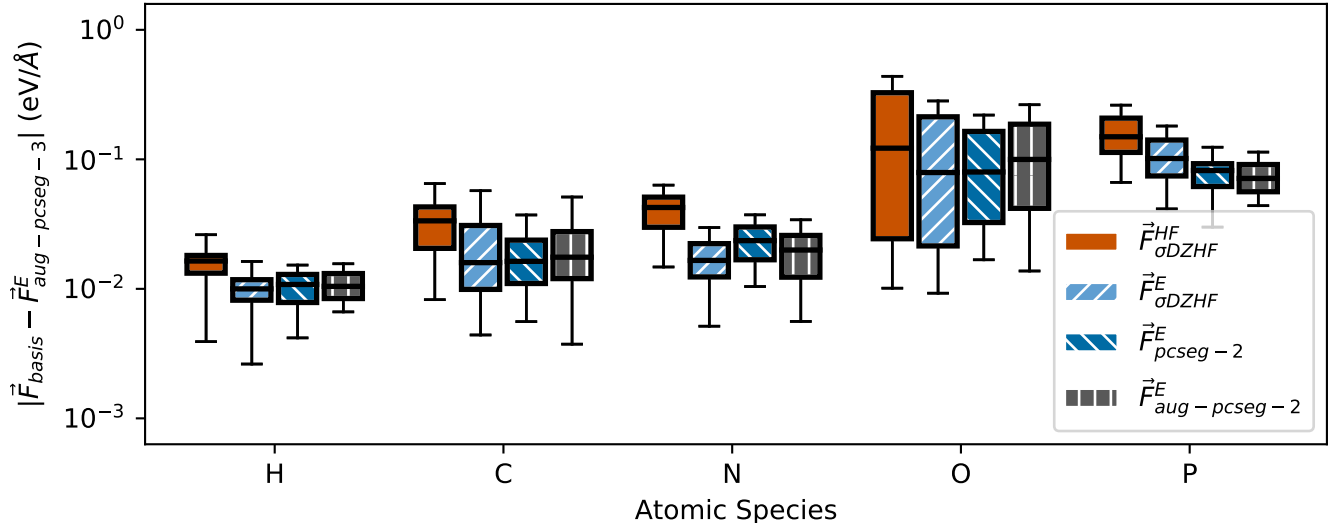


FIG. 3. Error in the computed forces for the DNA structures, with the σ DZHF, pcseg-2 and aug-pcseg-2 basis sets. The reference force was computed using the aug-pcseg-3 basis with the analytic force technique with RMS magnitudes 0.82 eV/Å, 5.33 eV/Å, 5.56 eV/Å, 4.41 eV/Å and 16.26 eV/Å for the H, C, N, O and P atoms respectively.

System	Optim.	$ d - d_{\text{ref}} $ (mÅ)	$ \theta - \theta_{\text{ref}} $ (°)	$ \phi - \phi_{\text{ref}} $ (°)
		Min — Max	Min — Max	Min — Max
water	$\vec{F}_{\text{pcseg-2}}^E$	0.017 — 0.017	0.045 — 0.045	
	$\vec{F}_{\sigma\text{DZHF}}^{\text{HF}}$	0.579 — 0.579	0.123 — 0.123	
ammonia	$\vec{F}_{\text{pcseg-2}}^E$	0.247 — 0.247	0.230 — 0.230	
	$\vec{F}_{\sigma\text{DZHF}}^{\text{HF}}$	0.707 — 0.707	0.228 — 0.228	
ethane	$\vec{F}_{\text{pcseg-2}}^E$	0.369 — 0.504	0.004 — 0.004	0.0001 — 0.0001
	$\vec{F}_{\sigma\text{DZHF}}^{\text{HF}}$	0.462 — 1.334	0.009 — 0.010	0.0001 — 0.0001
acetylene	$\vec{F}_{\text{pcseg-2}}^E$	0.216 — 0.696		
	$\vec{F}_{\sigma\text{DZHF}}^{\text{HF}}$	0.207 — 0.695		
allene	$\vec{F}_{\text{pcseg-2}}^E$	0.238 — 0.410	0.001 — 0.037	0.0001 — 0.0001
	$\vec{F}_{\sigma\text{DZHF}}^{\text{HF}}$	0.451 — 0.727	0.001 — 0.003	0.0001 — 0.0002
methylamine	$\vec{F}_{\text{pcseg-2}}^E$	0.126 — 0.443	0.016 — 0.066	0.001 — 0.049
	$\vec{F}_{\sigma\text{DZHF}}^{\text{HF}}$	0.306 — 1.985	0.023 — 0.084	0.001 — 0.025
hydroxysulphane	$\vec{F}_{\text{pcseg-2}}^E$	0.021 — 5.756	0.226 — 0.326	0.490 — 0.490
	$\vec{F}_{\sigma\text{DZHF}}^{\text{HF}}$	0.516 — 11.217	0.196 — 0.600	0.676 — 0.676
ethanol	$\vec{F}_{\text{pcseg-2}}^E$	0.093 — 0.415	0.002 — 0.087	0.0001 — 0.049
	$\vec{F}_{\sigma\text{DZHF}}^{\text{HF}}$	0.137 — 3.606	0.001 — 0.216	0.0001 — 0.118

TABLE III. Errors for optimized geometries using HF gradients with the σ DZHF basis ($\vec{F}_{\sigma\text{DZHF}}^{\text{HF}}$) or analytic gradients with the pcseg-2 basis ($\vec{F}_{\text{pcseg-2}}^E$). All errors are relative to a reference geometry optimized with analytic gradients and the pcseg-4 basis. Three error metrics are shown: distances between bonded atoms d in Å, angles between bonded atoms θ in degrees, and dihedral angles ϕ in degrees. The minimum and maximum absolute errors in all three metrics relative to the reference geometry are provided. Linear molecules have no data for θ , and most simple molecules have no data for ϕ .

yield smaller errors at lower computational costs for the present purposes of reproducing DFT forces, following the rationale for the polarization consistent basis sets of Jensen⁵². Alternatively, the design of the σ NZ basis sets could be revisited by adding more functions.

As a final point, we note that the error distribution for oxygen is considerably wider than that for the other atoms. This can be tentatively explained by the wider range of environments for oxygen in the DNA structures: there is neutral O⁰ in the A, C, G and T bases and a neg-

atively charged O^- anion in the phosphate group, while the H, C, N and P atoms are only found in their electrically neutral forms in DNA.⁵³

D. Geometry optimization with HF forces

To demonstrate the usefulness of HF forces, we run geometry optimization on the benchmark set of molecules of section IV B using both HF forces and analytic forces. The starting geometry for all calculations is the non-equilibrium geometry for which forces were calculated in section IV B. For comparison, reference geometries were optimized using analytic forces with the pcseg-4 basis. We emphasize an important point: geometry optimization using HF forces makes no use of analytic forces, neither in generating the geometry updates, nor in the convergence criteria.

The results of geometry optimization are presented in Tab. III. For each system, we compare two different geometries: an optimized geometry using pcseg-2 analytic forces $\vec{F}_{\text{pcseg-2}}^E$, and an optimized geometry using the σ DZHF basis and HF forces $\vec{F}_{\sigma\text{DZHF}}^{\text{HF}}$. We then compute three different metrics comparing the geometry to the reference optimized geometry.

The first metric, $|d - d_{\text{ref}}|$ presents the absolute error in pairwise distances for bonded atoms in a given geometry, d relative to the reference geometry d_{ref} . To compute this metric we take the given geometry and compute a list of pairwise distances between all pairs of bonded atoms. An absolute difference between this list of distances and a similar list for the reference geometry is computed, and the minimum and maximum absolute errors in mÅ are reported. The second metric, $|\theta - \theta_{\text{ref}}|$ follows a similar philosophy, where we compute a list of angles between bonded atoms for a given geometry and the reference geometry, θ and θ_{ref} , and we report again the minimum and maximum absolute difference in degrees. Finally, we have the third metric $|\phi - \phi_{\text{ref}}|$, where we compute all dihedral angles for a given geometry and the reference, ϕ and ϕ_{ref} , and report the minimum and absolute difference in degrees.

We begin with geometries optimized with analytic gradients and the pcseg-2 basis. Pairwise distances agree with the reference within 1 mÅ, with the only exceptional outlier being hydroxysulphane (HSOH) with a 5.756 mÅ error for the S–O bond, constituting a small 0.38% error in the bond length. For angles, both bonding θ and dihedrals ϕ , we find agreement with the reference geometry within a few tenths of a degree, the largest differences being observed in the angles for hydroxysulphane that cap out at 0.490 degrees error in the dihedral angle.

We move next to geometries computed using the σ DZHF basis and HF forces, which are remarkably accurate. Perhaps as expected, geometries optimized using the σ DZHF basis with HF forces yield slightly (2–3 times) larger errors across the board compared to geometries optimized using analytic forces. Nonetheless, general trends

for the optimized geometries using HF forces are promising. Bond lengths are accurate to a few mÅ, and bond and dihedral angles are accurate to a few tenths of a degree. We see then clearly that one can conduct state-of-the-art geometry optimization with HF forces using the σ DZHF basis for all molecules considered in this work.

E. Molecular dynamics with HF forces

As a final demonstration of the value of HF forces with the σ NZHF bases, we conduct a BOMD calculation in the NVE ensemble on a single ethanol molecule using HF forces in the MD integration. We use the starting configuration for ethanol from the benchmark set of molecules in section IV B and impart a randomized initial velocity on each atom in the molecule to provide an average temperature near 300K. The instantaneous temperature is calculated with the conventional formula

$$T(t) = \frac{2}{3(N_{\text{atom}} - 1)k_B} E_{\text{kin}}(t) \quad (6)$$

where E_{kin} is the kinetic energy of the molecule, N_{atom} is the total number of atoms, k_B the Boltzmann constant, and t is the time.

Fig. 4 shows times series data of the temperature and total energy of the MD calculations of ethanol using HF forces. As a point of comparison we also include MD simulations computed using analytic forces and the pcseg-2 basis, holding all other details of the MD calculation fixed. The temperature data shows typical fluctuations in time around a time series average temperature near $\langle T \rangle \sim 300$ K as expected.

More interesting is the total energy time series, which we plot as fluctuations around the time series average $\langle E \rangle$. Conceptually, the fluctuations present in the MD calculation with analytic forces arise from the finite timestep of 1 fs chosen in the Verlet integration. In addition to the finite timestep error, the MD calculation with HF forces has an additional source of total energy fluctuation arising from the HF forces not strictly satisfying momentum conservation discussed in section IV A, potentially leading to spontaneous heating within the simulation. For both calculations we find fluctuations in the total energy near 0.5 kcal/mol arising from the finite precision of the MD simulation, constituting a relative fluctuation near $10^{-4}\%$, alleviating concerns about erratic behavior in total energy for NVE BOMD calculations with HF forces.

Fig. 5 shows three snapshots of the ethanol molecule at 0 fs, 50 fs, and 100 fs from our MD calculations. We plot the configurations using a transformed set of coordinates, since some atoms in the ethanol have identical x, y coordinates and differ only in the z coordinate. The transformed coordinates are simply rotations in the $x - z$ and $y - z$ planes by an angle $\alpha = 5.73^\circ$ (0.1 rad), which was chosen for visual clarity. We find excellent agreement between the MD configurations generated using HF

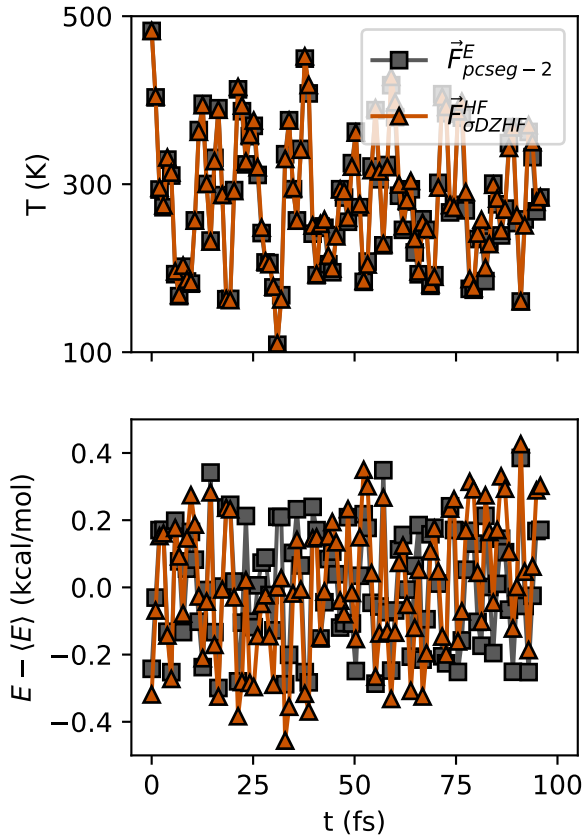


FIG. 4. Time series data of instantaneous temperature and total energy fluctuations in NVE BOMD simulations of ethanol. Two results are shown per figure, one for an MD simulation with analytic forces computed using the pcseg-2 basis ($\vec{F}_{pcseg-2}^E$) and one for an MD simulation with HF forces computed using HF forces and the σ DZHF basis ($\vec{F}_{\sigma DZHF}^E$). The time series averaged temperatures $\langle T \rangle$ for the pcseg-2 and σ DZHF calculations are 280.63 K and 283.76 K, and time series averaged energies $\langle E \rangle$, respectively, -97200.70 kcal/mol and -97207.26 kcal/mol.

forces with the σ DZHF basis and those generated with analytic forces and the pcseg-2 basis, further solidifying the potency of HF forces with the σ NZHF basis for accurate MD calculations. An animated version of the MD simulation with frames at each 1 fs timestep are provided in the Supplementary Material.

V. SUMMARY AND CONCLUSIONS

We constructed specially optimized basis sets named σ NZHF by systematically extending the family-style σ NZ basis sets,³¹ and demonstrated that the σ NZHF basis sets of this work successfully suppress the Pulay force in Gaussian basis set calculations. We used the σ NZHF basis sets to compute HF forces and optimize geometries of a large set of molecules, and found excellent agreement

with calculations using analytic forces and state-of-the-art pcseg-N Gaussian basis sets. Further, we ran a 100 fs BOMD simulation of an ethanol molecule using HF forces computed with the σ DZHF basis, and found that the configurations and total energies agreed well with a simulation with analytic forces computed with the pcseg-2 basis set.

Our results alleviate long-held concerns regarding the accuracy and efficiency of HF forces computed with atom-centered basis sets in applications like geometry optimization and MD.^{23,27} Additionally, by demonstrating that accurate forces can be computed just from an accurate electronic density in line with the Hohenberg–Kohn theorems,¹⁵ our work shines light on an interesting path for first principles ML force calculations. Instead of focusing on ML models that directly predict the force, one could train an ML density model on first principles densities computed with an appropriately optimized basis set like σ DZHF or σ TZHF. Forces can then be computed directly from the predicted ML density with the HF theorem (Eq. 2) and used in practical applications, such as geometry optimization and molecular dynamics. Such an application would enable accurate modeling for large-scale systems that are inaccessible to traditional first-principles techniques.

There are already many ML models which can accurately predict densities.^{54–56} However, these models typically predict the density in an auxiliary basis set. As such, the last major hurdle to integrating our accurate basis set to ML HF forces is the construction of optimized *auxiliary* basis sets according to the ordinary basis sets constructed in this work. With these optimized auxiliary basis sets in hand—which might be generated automatically⁵⁷—a promising pipeline would emerge for the accurate computation of forces for large-scale systems built on an ML model for the electronic density. We hope to follow up with work of this nature in the near future.

ACKNOWLEDGEMENTS

J.A.R., S.P., and A.J.L. were supported by the Harry S. Truman Fellowship, and the Laboratory Directed Research and Development and Academic Alliance Programs of Sandia National Laboratories. Sandia National Laboratories is a multimission laboratory managed and operated by National Technology & Engineering Solutions of Sandia, LLC, a wholly owned subsidiary of Honeywell International Inc., for the U.S. Department of Energy’s National Nuclear Security Administration under contract DE-NA0003525. We thank the Sandia Academic Alliance for supporting this work. S.L. acknowledges funding from the Academy of Finland through project numbers 350282 and 353749. We thank Sandia National Laboratories and the UNM Center for Advanced Research Computing, supported in part by the National Science Foundation, for providing the high performance computing and large-scale storage resources

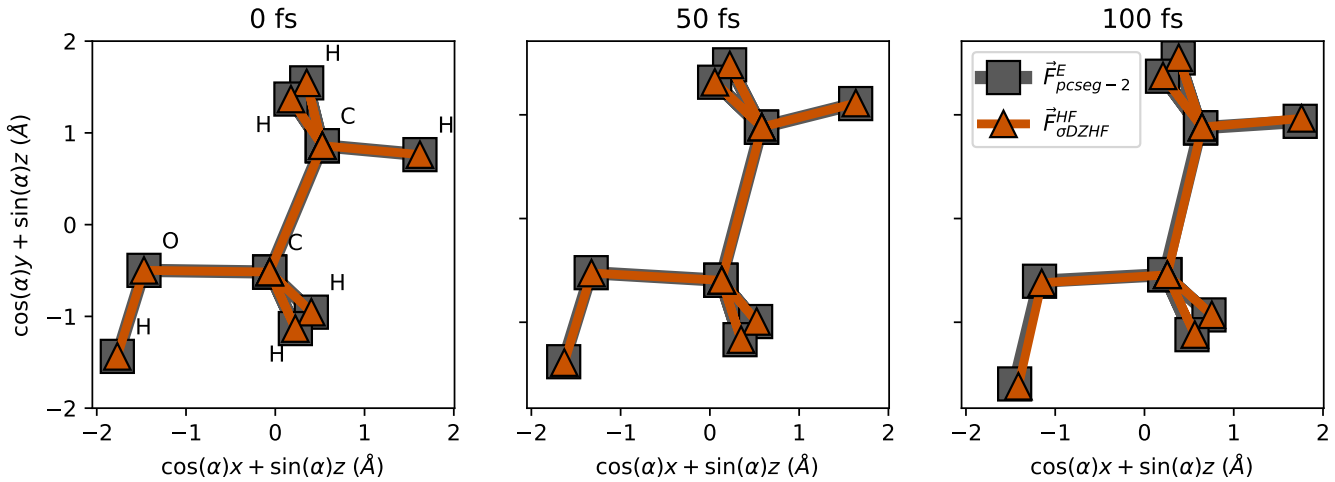


FIG. 5. Snapshots at 0, 50 and 100 fs comparing between NVE BOMD simulations of ethanol using analytic and HF derivatives. Transformed coordinates are used to visualize all the atoms in the ethanol molecule in a 2-d plane by rotating the x and y coordinates into the z plane via an angle $\alpha = 5.73^\circ$ (0.1 rad). A full animation of the MD simulations can be found in the Supplementary Material. (Multimedia view)

used in this work. This paper describes objective technical results and analysis. Any subjective views or opinions that might be expressed in the paper do not necessarily represent the views of the U.S. Department of Energy or the United States Government.

- ¹P. Carloni, U. Rothlisberger, and M. Parrinello, “The role and perspective of ab initio molecular dynamics in the study of biological systems,” *Acc. Chem. Res.* **35**, 455–464 (2002).
- ²R. J. Trabanino, S. E. Hall, N. Vaidehi, W. B. Floriano, V. W. Kam, and W. A. Goddard, “First principles predictions of the structure and function of G-protein-coupled receptors: Validation for bovine rhodopsin,” *Biophys. J.* **86**, 1904–1921 (2004).
- ³M. Iannuzzi, A. Laio, and M. Parrinello, “Efficient exploration of reactive potential energy surfaces using Car-Parrinello molecular dynamics,” *Phys. Rev. Lett.* **90**, 238302 (2003).
- ⁴J. Åqvist and A. Warshel, “Simulation of enzyme reactions using valence bond force fields and other hybrid quantum/classical approaches,” *Chem. Rev.* **93**, 2523–2544 (1993).
- ⁵F. L. Gervasio, P. Carloni, and M. Parrinello, “Electronic structure of wet DNA,” *Phys. Rev. Lett.* **89**, 108102 (2002).
- ⁶M. Elstner, P. Hobza, T. Frauenheim, S. Suhai, and E. Kaxiras, “Hydrogen bonding and stacking interactions of nucleic acid base pairs: A density-functional-theory based treatment,” *J. Chem. Phys.* **114**, 5149–5155 (2001).
- ⁷N. V. Dokholyan and E. I. Shakhnovich, “Understanding hierarchical protein evolution from first principles,” *J. Mol. Biol.* **312**, 289–307 (2001).
- ⁸S. Pathak, T. Rakib, R. Hou, A. Nevidomskyy, E. Ertekin, H. T. Johnson, and L. K. Wagner, “Accurate tight-binding model for twisted bilayer graphene describes topological flat bands without geometric relaxation,” *Phys. Rev. B* **105**, 115141 (2022).
- ⁹K. Uchida, S. Furuya, J.-I. Iwata, and A. Oshiyama, “Atomic corrugation and electron localization due to Moiré patterns in twisted bilayer graphenes,” *Phys. Rev. B* **90**, 155451 (2014).
- ¹⁰S. Fang and E. Kaxiras, “Electronic structure theory of weakly interacting bilayers,” *Phys. Rev. B* **93**, 235153 (2016).
- ¹¹G. Cantele, D. Alfe, F. Conte, V. Cataudella, D. Ninno, and P. Lucignano, “Structural relaxation and low-energy properties of twisted bilayer graphene,” *Phys. Rev. Research* **2**, 043127 (2020).
- ¹²J. C. A. Prentice, J. Aarons, J. C. Womack, A. E. A. Allen, L. Andrinopoulos, L. Anton, R. A. Bell, A. Bhandari, G. A. Bramley, R. J. Charlton, R. J. Clements, D. J. Cole, G. Constantinescu, F. Corsetti, S. M.-M. Dubois, K. K. B. Duff, J. M. Escartín, A. Greco, Q. Hill, L. P. Lee, E. Linscott, D. D. O’Regan, M. J. S. Phipps, L. E. Ratcliff, A. R. Serrano, E. W. Tait, G. Teobaldi, V. Vitale, N. Yeung, T. J. Zuehlsdorff, J. Dziedzic, P. D. Haynes, N. D. M. Hine, A. A. Mostofi, M. C. Payne, and C.-K. Skylaris, “The ONETEP linear-scaling density functional theory program,” *J. Chem. Phys.* **152**, 174111 (2020).
- ¹³S. Mohr, L. E. Ratcliff, L. Genovese, D. Caliste, P. Boulanger, S. Goedecker, and T. Deutsch, “Accurate and efficient linear scaling DFT calculations with universal applicability,” *Phys. Chem. Chem. Phys.* **17**, 31360–31370 (2015).
- ¹⁴Z. Luo, X. Qin, L. Wan, W. Hu, and J. Yang, “Parallel implementation of large-scale linear scaling density functional theory calculations with numerical atomic orbitals in HONPAS,” *Frontiers in Chemistry* **8** (2020), 10.3389/fchem.2020.589910.
- ¹⁵P. Hohenberg and W. Kohn, “Inhomogeneous electron gas,” *Phys. Rev.* **136**, B864–B871 (1964).
- ¹⁶W. Kohn and L. J. Sham, “Self-consistent equations including exchange and correlation effects,” *Phys. Rev.* **140**, A1133–A1138 (1965).
- ¹⁷V. Botu, R. Batra, J. Chapman, and R. Ramprasad, “Machine learning force fields: Construction, validation, and outlook,” *J. Phys. Chem. C* **121**, 511–522 (2017).
- ¹⁸J. Behler, “Perspective: Machine learning potentials for atomistic simulations,” *J. Chem. Phys.* **145**, 170901 (2016).
- ¹⁹C. M. Handley and J. Behler, “Next generation interatomic potentials for condensed systems,” *Eur. Phys. J. B* **87**, 152 (2014).
- ²⁰P. Pulay, “Ab initio calculation of force constants and equilibrium geometries in polyatomic molecules,” *Mol. Phys.* **17**, 197–204 (1969).
- ²¹R. Assaraf and M. Caffarel, “Computing forces with quantum Monte Carlo,” *J. Chem. Phys.* **113**, 4028–4034 (2000).
- ²²M. Casalegno, M. Mella, and A. M. Rappe, “Computing accurate forces in quantum Monte Carlo using Pulay’s corrections and energy minimization,” *J. Chem. Phys.* **118**, 7193–7201 (2003).
- ²³P. Pulay, “Direct use of the gradient for investigating molecular energy surfaces,” in *Applications of Electronic Structure Theory*, edited by H. F. Schaefer (Springer US, Boston, MA, 1977) pp. 153–185.
- ²⁴H. Nakatsuji, K. Kanda, and T. Yonezawa, “Force in SCF theories,” *Chemical Physics Letters* **75**, 340–346 (1980).

- ²⁵H. Nakatsuji, T. Hayakawa, and M. Hada, "Force in SCF theories. MC SCF and open-shell RHF theories," *Chem. Phys. Lett.* **80**, 94–100 (1981).
- ²⁶H. Nakatsuji, K. Kanda, M. Hada, and T. Yonezawa, "Force in SCF theories. test of the new method," *The Journal of Chemical Physics* **77**, 3109–3122 (1982), <https://doi.org/10.1063/1.444234>.
- ²⁷P. Pulay, "Comment on "Force in SCF theories"," *The Journal of Chemical Physics* **79**, 2491–2492 (1983), <https://doi.org/10.1063/1.446089>.
- ²⁸H. Nakatsuji, K. Kanda, M. Hada, and T. Yonezawa, "Reply to "Comment on 'Force in SCF theories'"," *J. Chem. Phys.* **79**, 2493–2495 (1983).
- ²⁹J. F. Rico, R. López, I. Ema, and G. Ramírez, "Generation of basis sets with high degree of fulfillment of the Hellmann–Feynman theorem," *J. Comput. Chem.* **28**, 748–758 (2007).
- ³⁰J. Baker, "Techniques for geometry optimization: A comparison of cartesian and natural internal coordinates," *Journal of Computational Chemistry* **14**, 1085–1100 (1993), <https://onlinelibrary.wiley.com/doi/pdf/10.1002/jcc.540140910>.
- ³¹I. Ema, G. Ramírez, R. López, and J. M. G. de la Vega, "Sigma basis sets: a new family of gto basis sets for molecular calculations," (2022).
- ³²F. Jensen, "Unifying general and segmented contracted basis sets. segmented polarization consistent basis sets," *J. Chem. Theory Comput.* **10**, 1074–1085 (2014).
- ³³T. H. Dunning, "Gaussian basis sets for use in correlated molecular calculations. I. The atoms boron through neon and hydrogen," *J. Chem. Phys.* **90**, 1007–1023 (1989).
- ³⁴B. P. Pritchard, D. Altarawy, B. Didier, T. D. Gibson, and T. L. Windus, "New basis set exchange: An open, up-to-date resource for the molecular sciences community," *J. Chem. Inf. Model.* **59**, 4814–4820 (2019), pMID: 31600445, <https://doi.org/10.1021/acs.jcim.9b00725>.
- ³⁵K. L. Schuchardt, B. T. Didier, T. Elsethagen, L. Sun, V. Gummoothi, J. Chase, J. Li, and T. L. Windus, "Basis set exchange: A community database for computational sciences," *J. Chem. Inf. Model.* **47**, 1045–1052 (2007), pMID: 17428029, <https://doi.org/10.1021/ci600510j>.
- ³⁶M. Ernzerhof and G. E. Scuseria, "Assessment of the Perdew–Burke–Ernzerhof exchange-correlation functional," *J. Chem. Phys.* **110**, 5029–5036 (1999).
- ³⁷C. Adamo and V. Barone, "Toward reliable density functional methods without adjustable parameters: The PBE0 model," *J. Chem. Phys.* **110**, 6158–6170 (1999).
- ³⁸S. Lehtola, C. Steigemann, M. J. Oliveira, and M. A. Marques, "Recent developments in libxc — A comprehensive library of functionals for density functional theory," *SoftwareX* **7**, 1–5 (2018).
- ³⁹D. G. A. Smith, L. A. Burns, A. C. Simmonett, R. M. Parrish, M. C. Schieber, R. Galvelis, P. Kraus, H. Kruse, R. Di Remigio, A. Alenaizan, A. M. James, S. Lehtola, J. P. Misiewicz, M. Scheurer, R. A. Shaw, J. B. Schriber, Y. Xie, Z. L. Glick, D. A. Sirianni, J. S. O'Brien, J. M. Waldrop, A. Kumar, E. G. Hohenstein, B. P. Pritchard, B. R. Brooks, H. F. Schaefer, A. Y. Sokolov, K. Patkowski, A. E. DePrince, U. Bozkaya, R. A. King, F. A. Evangelista, J. M. Turney, T. D. Crawford, and C. D. Sherrill, "PSI4 1.4: Open-source software for high-throughput quantum chemistry," *J. Chem. Phys.* **152**, 184108 (2020).
- ⁴⁰Q. Sun, T. C. Berkelbach, N. S. Blunt, G. H. Booth, S. Guo, Z. Li, J. Liu, J. D. McClain, E. R. Sayfutyarova, S. Sharma, S. Wouters, and G. K.-L. Chan, "Pyscf: the python-based simulations of chemistry framework," *WIREs Computational Molecular Science* **8**, e1340 (2018), <https://wires.onlinelibrary.wiley.com/doi/pdf/10.1002/wcms.1340>.
- ⁴¹Q. Sun, X. Zhang, S. Banerjee, P. Bao, M. Barbry, N. S. Blunt, N. A. Bogdanov, G. H. Booth, J. Chen, Z.-H. Cui, J. J. Eriksen, Y. Gao, S. Guo, J. Hermann, M. R. Hermes, K. Koh, P. Koval, S. Lehtola, Z. Li, J. Liu, N. Mardirossian, J. D. McClain, M. Motta, B. Mussard, H. Q. Pham, A. Pulkin, W. Purwanto, P. J. Robinson, E. Ronca, E. R. Sayfutyarova, M. Scheurer, H. F. Schurkus, J. E. T. Smith, C. Sun, S.-N. Sun, S. Upadhyay, L. K. Wagner, X. Wang, A. White, J. D. Whitfield, M. J. Williamson, S. Wouters, J. Yang, J. M. Yu, T. Zhu, T. C. Berkelbach, S. Sharma, A. Y. Sokolov, and G. K.-L. Chan, "Recent developments in the pyscf program package," *The Journal of Chemical Physics* **153**, 024109 (2020), <https://doi.org/10.1063/5.0006074>.
- ⁴²F. Weigend, "Hartree–Fock exchange fitting basis sets for H to Rn," *J. Comput. Chem.* **29**, 167–175 (2008).
- ⁴³L.-P. Wang and C. Song, "Geometry optimization made simple with translation and rotation coordinates," *The Journal of Chemical Physics* **144**, 214108 (2016), <https://doi.org/10.1063/1.4952956>.
- ⁴⁴L. Verlet, "Computer "experiments" on classical fluids. I. thermodynamical properties of lennard-jones molecules," *Phys. Rev.* **159**, 98–103 (1967).
- ⁴⁵A. J. Lee, J. A. Rackers, and W. P. Bricker, "Predicting accurate ab initio DNA electron densities with equivariant neural networks," *Biophysical Journal* (2022), <https://doi.org/10.1016/j.bpj.2022.08.045>.
- ⁴⁶D. Case, H. Aktulga, K. Belfon, I. Ben-Shalom, S. Brozell, D. Cerutti, I. T.E. Cheatham, G. Cisneros, V. Cruzeiro, T. Darden, R. Duke, G. Giambasu, M. Gilson, H. Gohlke, A. Goetz, R. Harris, S. Izadi, S. Izmailov, C. Jin, K. Kasavajhala, M. Kaymak, E. King, A. Kovalenko, T. Kurtzman, T. Lee, S. LeGrand, P. Li, C. Lin, J. Liu, T. Luchko, R. Luo, M. Machado, V. Man, M. Manathunga, K. Merz, Y. Miao, O. Mikhailovskii, G. Monard, H. Nguyen, K. O'Hearn, A. Onufriev, F. Pan, S. Pantano, R. Qi, A. Rahnamoun, D. Roe, A. Roitberg, C. Sagui, S. Schott-Verdugo, J. Shen, C. Simmerling, N. Skrynnikov, J. Smith, J. Swails, R. Walker, J. Wang, H. Wei, R. Wolf, X. Wu, Y. Xue, D. York, S. Zhao, and P. Kollman, "Amber 2021," University of California, San Francisco (2021).
- ⁴⁷I. Ivani, P. D. Dans, A. Noy, A. Pérez, I. Faustino, A. Hospital, J. Walther, P. Andrio, R. Goñi, A. Balaceanu, G. Portella, F. Battistini, J. L. Gelpí, C. González, M. Vendruscolo, C. A. Laughon, S. A. Harris, D. A. Case, and M. Orozco, "Parmbsc1: A refined force-field for DNA simulations," *Nat. Methods* **13**, 55–58 (2016).
- ⁴⁸T. J. Richmond and C. A. Davey, "The structure of DNA in the nucleosome core," *Nature* **423**, 145–150 (2003).
- ⁴⁹W. L. Jorgensen, J. Chandrasekhar, and J. D. Madura, "Comparison of simple potential functions for simulating liquid water," *J. Chem. Phys.* **79**, 926 (1983).
- ⁵⁰P. Jurečka, J. Sponer, J. Černý, and P. Hobza, "Benchmark database of accurate (MP2 and CCSD(T) complete basis set limit) interaction energies of small model complexes, DNA base pairs, and amino acid pairs," *Phys. Chem. Chem. Phys.* **8**, 1985–1993 (2006).
- ⁵¹P. Hobza and J. Sponer, "Toward true DNA base-stacking energies: MP2, CCSD(T), and complete basis set calculations," *J. Am. Chem. Soc.* **124**, 11802–11808 (2002).
- ⁵²F. Jensen, "Polarization consistent basis sets: Principles," *J. Chem. Phys.* **115**, 9113–9125 (2001).
- ⁵³J. D. Watson and F. H. C. Crick, "Molecular structure of nucleic acids: A structure for deoxyribose nucleic acid," *Nature* **171**, 737–738 (1953).
- ⁵⁴A. Grisafi, A. Fabrizio, B. Meyer, D. M. Wilkins, C. Corminboeuf, and M. Ceriotti, "Transferable machine-learning model of the electron density," *ACS Cent. Sci.* **5**, 57–64 (2019).
- ⁵⁵B. Cuevas-Zuviría and L. F. Pacios, "Machine learning of analytical electron density in large molecules through message-passing," *J. Chem. Inf. Model.* **61**, 2658–2666 (2021).
- ⁵⁶J. A. Rackers, L. Tecot, M. Geiger, and T. E. Smidt, "Cracking the quantum scaling limit with machine learned electron densities," (2022).
- ⁵⁷S. Lehtola, "Straightforward and accurate automatic auxiliary basis set generation for molecular calculations with atomic orbital basis sets," *J. Chem. Theory Comput.* **17**, 6886–6900 (2021).

Supplemental Materials: Accurate Hellmann–Feynman forces with optimized atom-centered Gaussian basis sets in density functional theory

I. DEFINITIONS

Gaussian primitive functions (pGTO) are defined as the product of a Gaussian radial factor, $e^{-\xi r^2}$, and an angular factor that can be either a product of powers of Cartesian coordinates, or a regular spherical harmonic.

In this work, we will use normalized spherical pGTO, g_{lm} , defined as:

$$g_{lm}(\xi, \mathbf{r}) = \mathcal{N}_{l,\xi}^r \mathcal{N}_{lm}^{\Omega} e^{-\xi r^2} z_l^m(\mathbf{r}) \quad (7)$$

where $z_l^m(\mathbf{r})$ are unnormalized regular solid harmonics:

$$z_l(\mathbf{r}) = r^l (-1)^l P_l^{|m|}(\cos \theta) \begin{cases} \cos m\phi & (m \geq 0) \\ \sin |m|\phi & (m < 0) \end{cases} \quad (8)$$

and \mathcal{N}_{ξ} and $\mathcal{N}_{LM}^{\Omega}$ are the radial and angular normalization constants given by:

$$\mathcal{N}_{l,\xi}^r = 2^{l+1} \sqrt{\frac{\xi^l}{(2l+1)!!}} \left[\frac{(2\xi)^3}{\pi} \right]^{1/4} \quad (9)$$

$$\mathcal{N}_{lm}^{\Omega} = \left[\frac{(2l+1) (l-|m|)!}{2(1+\delta_{m0}) \pi (l+|m|)!} \right]^{1/2} \quad (10)$$

Usual Gaussian basis sets consist of contractions (linear combinations) of Gaussian primitives. They are known as contracted Gaussian functions (GTO), G_{LM} , defined as:

$$G_{lm}(\mathbf{r}) = \sum_{i=1}^{N_G} c_i g_{lm,i}(\mathbf{r}) \quad (11)$$

where i labels the primitives in the set, and the coefficients c_i are determined by different procedures subject to the normalization of the GTO. The number of coefficients and their values depend on the recipe used in the construction of a particular basis set.

Sigma basis sets (σ BS) are a particular type of GTO BS in which if a given primitive appears multiplied by a spherical harmonic of quantum number $l = L$, then functions with the same exponent are also present for $0 \leq l < L$. This is an interesting property for the development of atomic BS with a high degree of fulfillment of the Hellmann–Feynman theorem (BSHF), as will be shown later.

II. DISTANCE BETWEEN BASIS SETS

In the comparison of basis sets, it is very useful to consider the distance between the subspaces generated by them. Let \mathcal{V}_1 and \mathcal{V}_2 be two subspaces of the real Hilbert space generated by two GTO basis sets, $\{G_i^{(1)}\}_{i=1}^{N_G^{(1)}}$ and $\{G_i^{(2)}\}_{i=1}^{N_G^{(2)}}$. It has been proved⁷ that there exist orthonormal basis sets $\{\tilde{G}_i^{(1)}\}_{i=1}^{N_G^{(1)}}$ and $\{\tilde{G}_i^{(2)}\}_{i=1}^{N_G^{(2)}}$, such that:

$$\begin{aligned} \langle \tilde{G}_i^{(1)} | \tilde{G}_j^{(1)} \rangle &= \delta_{ij} & \langle \tilde{G}_i^{(2)} | \tilde{G}_j^{(2)} \rangle &= \delta_{ij} \\ \langle \tilde{G}_i^{(1)} | \tilde{G}_j^{(2)} \rangle &= \lambda_i \delta_{ij} \end{aligned} \quad (12)$$

The orthonormal BS, \tilde{G} , are related to the original ones, G , by simple linear transformations:

$$\tilde{G}^{(1)} = \mathcal{D}^{(1)} \cdot G^{(1)} \quad \tilde{G}^{(2)} = \mathcal{D}^{(2)} \cdot G^{(2)} \quad (13)$$

The pairs of functions $\tilde{G}_i^{(1)}, \tilde{G}_i^{(2)}$ are *partners*, and the distance between them can be obtained as:

$$d_{ii} = |\tilde{G}_i^{(1)} - \tilde{G}_i^{(2)}| = \sqrt{2(1 - \lambda_i)} \quad (14)$$

These distances can be used to define the distance, Δ , between the subspaces. Among the possible definitions for this distance⁷, we choose:

$$\Delta^2 = \sum_i d_{ii}^2 \quad (15)$$

From eqs (14) and (15), it is clear that the closer the λ_i are to 1, the smaller the distance between the subspaces \mathcal{V}_1 and \mathcal{V}_2 . Thus, if both BS span the same subspace, all the λ_i are equal to 1 and the distance between them is zero.

III. DEVELOPMENT OF BASIS SETS USING A DISTANCE CRITERION

Let us consider a GTO BS, $G^{(1)}$, that we will call the *reference*, and the problem of developing an alternative BS, $G^{(2)}$, such that the distance between them is minimum. This can be useful, for instance, when $G^{(2)}$ is smaller than the reference $G^{(1)}$, but one wants to reproduce as much as possible the subspace spanned by $G^{(1)}$.

It has been proved⁷ that this can be done by defining the projector $\tilde{\mathbf{P}}^{(1)}$ onto \mathcal{V}_1 , whose matrix representation on the \mathcal{V}_2 subspace reads:

$$\mathbf{P}^{(1)} = ([\mathbf{S}^{(2)}]^{-1/2} \mathbf{M} \mathbf{C}) (\mathbf{C}^\dagger \mathbf{M}^\dagger [\mathbf{S}^{(2)}]^{-1/2}) \equiv \mathbf{M} \mathbf{M}^\dagger \quad (16)$$

where $\mathbf{S}^{(2)}$ is the overlap matrix in the subspace \mathcal{V}_2 generated by $G^{(2)}$ and \mathbf{M} is the mixed overlap matrix between elements of \mathcal{V}_2 and \mathcal{V}_1 , whose elements are given respectively by:

$$S_{ij} = \langle G_i^{(2)} | G_j^{(2)} \rangle \quad \text{and} \quad M_{ij} = \langle G_i^{(2)} | G_j^{(1)} \rangle \quad (17)$$

and \mathbf{C} is the coefficient matrix that defines an orthonormal set of functions, $G^{ON(1)}$, in \mathcal{V}_1 :

$$G_i^{ON(1)} = \sum_r G_r^{(1)} C_{ri} \quad (18)$$

It should be noticed that the matrix \mathbf{M} is not symmetric, even it can be non square. However, the $\mathbf{P}^{(1)}$ is a symmetric square matrix. Diagonalizing $\mathbf{P}^{(1)}$ by a suitable unitary transformation, \mathbf{R} , one obtains the λ_i as the square root of the eigenvalues:

$$\mathbf{R}^\dagger \mathbf{P}^{(1)} \mathbf{R} = \Lambda_d^2 \quad (19)$$

with $\lambda_i = \Lambda_{ii}$ being the elements of the diagonal matrix Λ_d . The partner basis of the spaces are given by⁷ :

$$\tilde{G}_i^{(2)} = \sum_{r=1}^{N_G^{(2)}} G_r^{(2)} ([\mathbf{S}^{(2)}]^{-1/2} \mathbf{R})_{ri} \quad (20)$$

$$\tilde{G}_i^{(1)} = \lambda_i \sum_{r=1}^{N_G^{(1)}} G_r^{(1)} (\mathbf{C} \mathbf{M}^\dagger \mathbf{R})_{ri} \quad (21)$$

IV. OVERLAP BETWEEN GAUSSIAN FUNCTIONS AND THEIR DERIVATIVES.

In the application of the procedure described in sec III to the development of atomic BSHF, the reference BS is taken as a σ BS plus the derivatives of its functions with respect to the space coordinates. Therefore, overlap involving GTO and their derivatives are required. As GTO are linear combinations of primitive pGTO, the integrals involving the former can be obtained as linear combinations of integrals among the latter.

Due to the orthogonality of the pGTO with different M quantum numbers and given the symmetry in atoms, it is sufficient to consider the first derivatives with respect to Z , the remaining integrals involving derivatives to X or to Y being equal to them.

Let us consider first the derivative of a pGTO with respect to Z Cartesian coordinate, given by:

$$\frac{\partial g_{lm}(\xi, \mathbf{r})}{\partial Z} = \mathcal{N}_{l,\xi}^r \mathcal{N}_{lm}^\Omega \left[(l + |m|) z_{l-1}^m(\mathbf{r}) \left(1 - \frac{2\xi r^2}{2l+1} \right) - \frac{(l+1-|m|)}{2l+1} 2\xi z_{l+1}^m(\mathbf{r}) \right] e^{-\xi r^2} \quad (22)$$

As it can be seen, this derivative yields functions with $l-1$ and $l+1$ and the same exponent as the original pGTO. This fact makes σ BS specially useful for the development of Hellmann-Feynman BS (σ BSHF), as the introduction of the derivatives does not increase the number of pGTO in the basis set as much as with usual GTO BS. It is also important to note that the functions with $l-1$ contain an extra r^2 factor that it is not included in the functions of the σ BSHF.

The different types of overlap integrals required to build matrices \mathbf{S} and \mathbf{M} and to orthogonalize the $G^{(1)}$ functions, can be obtained with the aid of:

$$\int_0^\infty dr r^{2l+2} e^{-(\alpha+\beta)r^2} = \frac{(l+1/2)!}{2(\alpha+\beta)^{l+3/2}} \quad (23)$$

and

$$\int_0^\pi d\theta \sin(\theta) \int_0^{2\pi} d\phi z_l(\mathbf{r}) z_{l'}^{m'}(\mathbf{r}) = \delta_{ll'} \delta_{mm'} r^{2l} \frac{2(1+\delta_{m0}) \pi (l+|m|)!}{(2l+1) (l-|m|)!} \quad (24)$$

Thus, the overlap integral of a pair of pGTO is given by:

$$\langle g_{lm}(\xi) | g_{l'm'}(\xi') \rangle = \mathcal{N}_{l,\xi}^r \mathcal{N}_{l',\xi'}^r \mathcal{N}_{lm}^\Omega \mathcal{N}_{l'm'}^\Omega \delta_{ll'} \delta_{mm'} \frac{2(1+\delta_{m0}) \pi (l+|m|)!}{(2l+1) (l-|m|)!} \frac{(l+1/2)!}{2(\xi+\xi')^{l+3/2}} \quad (25)$$

the integral involving a pGTO and the derivative of a pGTO with respect to Z , by

$$\begin{aligned} \left\langle \frac{\partial}{\partial Z} g_{lm}(\xi) \middle| g_{l'm'}(\xi') \right\rangle &= \mathcal{N}_{l,\xi}^r \mathcal{N}_{l',\xi'}^r \mathcal{N}_{lm}^\Omega \mathcal{N}_{l'm'}^\Omega \delta_{mm'} \frac{2(1+\delta_{m0}) \pi (l'+|m|)!}{(2l'+1) (l'-|m|)!} \\ &\times \frac{(l'+1/2)!}{2(\xi+\xi')^{l'+3/2}} \left\{ \delta_{l-1,l'} (l+|m|) \frac{\xi'}{\xi+\xi'} - \delta_{l+1,l'} 2\xi \frac{(l+1-|m|)}{2l+1} \right\} \end{aligned} \quad (26)$$

and the integrals involving the derivatives with respect to Z of two pGTO, by:

$$\begin{aligned} \left\langle \frac{\partial}{\partial Z} g_{lm}(\xi) \middle| \frac{\partial}{\partial Z} g_{l'm'}(\xi') \right\rangle &= \mathcal{N}_{l,\xi}^r \mathcal{N}_{l',\xi'}^r \mathcal{N}_{lm}^\Omega \mathcal{N}_{l'm'}^\Omega \delta_{mm'} 2(1+\delta_{m0}) \pi \\ &\times \left\{ \frac{(l+|m|)!}{(2l-1) (l-1-|m|)!} \frac{(l-1/2)!}{2(\xi+\xi')^{l+3/2}} \right. \\ &\times \left[\delta_{ll'} (1 - \delta_{l,|m|}) (l+|m|) \frac{2l+3}{2l+1} \frac{\xi \xi'}{\xi+\xi'} - \delta_{l-1,l'+1} \frac{(l'+1-|m|) 2\xi'^2}{(2l'+1)} \right] \\ &+ \frac{(l+1+|m|)!}{(2l+3) (l-|m|)!} \frac{(l+3/2)!}{2(\xi+\xi')^{l+5/2}} \\ &\times \left. \left[-\delta_{l+1,l'-1} \frac{(l'+|m|) 2\xi^2}{(2l+1) (\xi+\xi')} + \delta_{ll'} \frac{(l+1-|m|) 4\xi \xi'}{(2l+1)^2} \right] \right\} \end{aligned} \quad (27)$$

V. CONSTRUCTION OF HELLMANN-FEYNMAN BASIS SETS

To develop a BS with a high degree of fulfillment of the Hellmann-Feynman theorem, we start choosing the set of pGTO corresponding to a σ BS of a given quality (σ NZ), and extend it with the functions corresponding to their derivatives. As eq (22) shows, the derivative of a pGTO with a given $l > 0$ yields three functions with the same exponent as in the pGTO: one function corresponds to $l+1$, and the other two to $l-1$, one of them bearing a factor r^2 . As in usual GTO BS no power of r is included in the primitives, we remove the functions with r^2 from the set, yielding what we call a *reduced set* of primitives, which will span the *reduced space*.

Next, we consider the contractions of the σ BS and their derivatives, which form the *reference set*, and try to reproduce the space spanned by them, the *reference space*, in the reduced space. For this purpose, we compute the distance between the reference and reduced spaces, as indicated in section III. If the distance is lower than a given threshold, that we take as 10^{-3} , the reduced space is considered sufficient to expand the contractions and their derivatives for practical purposes. If it is higher than this threshold, more primitives are added to the *reduced set* of

TABLE IV. Number of primitives and contracted basis functions. Functions marked with an asterisk * contain an r^2 factor.

Basis	# σ Exp.	# Primitives	# Contracted	# Contracted + derivatives ^a
H atom				
σ SZ	10	10 (10s)	1 [1s]	4 [1s, 1p]
σ DZ	10	19 (10s, 3p)	5 [2s, 1p]	18 [3s+1s*, 3p, 1d]
σ TZ	10	37 (10s, 4p, 3d)	14 [3s, 2p, 1d]	50 [5s+2s*, 6p+1p*, 3d, 1f]
σ SZHF	10	40 (10s, 10p)	4 [1s, 1p]	
σ DZHF	10	55 (10s, 10p, 3d)	17 [3s, 3p, 1d]	
σ TZHF	12	85 (11s, 11p, 4d, 3f)	46 [6s, 6p, 3d, 1f]	
C,N,O and F atoms				
σ SZ	15	45 (15s, 10p)	5 [2s, 1p]	18 [3s+1s*, 3p, 1d]
σ DZ	15	60 (15s, 10p, 3d)	14 [3s, 2p, 1d]	50 [5s+2s*, 6p+1p*, 3d, 1f]
σ TZ	15	86 (15s, 10p, 4d, 3f)	30 [4s, 3p, 2d, 1f]	108 [7s+3s*, 9p+2p*, 6d+1d*, 3f, 1g]
σ SZHF	15	110 (15s, 15p, 10d)	17 [3s, 3p, 1d]	
σ DZHF	15	131 (15s, 15p, 10d, 3f)	46 [6s, 6p, 3d, 1f]	
σ TZHF	15	169 (16s, 16p, 10d, 4f, 3g)	87 [8s, 8p, 5d, 3f, 1g]	
P,S and Cl atoms				
σ SZ	19	79 (19s, 15p)	9 [3s, 2p]	32 [5s+2s*, 5p, 2d]
σ DZ	19	79 (19s, 15p, 3d)	18 [4s, 3p, 1d]	64 [7s+3s*, 8p+1p*, 4d, 1f]
σ TZ	19	95 (19s, 15p, 4d, 3f)	34 [5s, 4p, 2d, 1f]	122 [9s+4s*, 11p+2p*, 7d+1d*, 3f, 1g]
σ SZHF	19	113 (19s, 19p, 15d)	30 [5s, 5p, 2d]	
σ DZHF	19	134 (19s, 19p, 15d, 3f)	59 [8s, 8p, 4d, 1f]	
σ TZHF	21	187 (20s, 20p, 15d, 4f, 3g)	100 [10s, 10p, 6d, 3f, 1g]	

primitives until the test on distance is fulfilled. It is worth noticing that the extra primitives, when necessary, are required to remedy the lack of functions with the r^2 factor, and this provides a hint for their selection.

The process for choosing the extra primitives when required is essentially heuristic. Based on the fact that the r^2 factor in the derivatives is divided by $2l+1$, we guess that primitive functions with lower l values will be more effective. Likewise, as the r^2 factor *shifts* the function towards higher values of r than the pure exponential, we also guess that small exponents will be also advantageous in this respect. With these guidelines, we analyzed the σ TZHF of oxygen in which extra primitives are necessary. A first attempt was made by adding a single s function followed by exponent optimization for reducing the distance. As this attempt and the addition of a second s function failed, a pair s, p was tried. In this case, after exponents optimization (without restrictions) this combination was successful. The process was repeated with other atoms and we found that, in the atoms treated so far (see Table IV) the addition of this pair of functions, with exponents optimized for each atom, was sufficient to get a distance below the selected threshold.

Once the *reduced set* has been completed, we carry out an expansion of the functions of the reference set in an orthogonal basis of the reduced set, that we will call *reduced contractions*. The process could end here, but we have noticed that choosing suitable orthogonal functions in the reduced set, the number of contractions necessary to satisfactorily expand the functions of the reference set can be further reduced. The selection of these contractions is made by computing the distance between the spaces spanned by subsets of reduced contractions and the reference space. This is accomplished in an iterative way, until a reduced subset fulfills the distance criterion. As it can be seen in Table IV, in case the σ TZHF of C, N, O, and F atoms, the GTO contractions plus their derivatives give 108 functions, whereas 87 functions are sufficient in the reduced subset to achieve the desired accuracy (distance). In case of P, S and Cl, the corresponding numbers for the σ TZHF are 122 and 100.

Finally, it is worth mentioning that the contractions added to the original σ BS to give the σ BSHF also affect the value of the energy (which will be lowered) and the wavefunction. This would lead to an endless optimization loop. Fortunately, the degree of fulfillment of the Hellmann-Feynman theorem achieved in the first iteration of the loop is sufficient for practical purposes, making it unnecessary to continue the process.